

**Role of Structural Organization in
the Urine Concentrating Mechanism of
An Avian Kidney***

Anita T. Layton

Address:

Department of Mathematics,

Duke University

Box 90320, Durham, NC 27708, U.S.A.

Telephone: (919) 660 6979

Facsimile: (919) 660 2821

Email: alayton@math.duke.edu

*This work was supported in part by the National Science Foundation,
grant DMS-0340654.

Abstract

The organization of tubules and blood vessels in the quail medullary cone is highly structured. This structural organization may result in preferential interactions among tubules and vessels, interactions that may enhance urine concentrating capability. In this study, we formulate a model framework for the urine concentrating mechanism of the quail kidney. The model simulates preferential interactions among renal tubules by representing two concentric cores and by specifying the fractions of tubules assigned to each of the concentric cores. The model equations are based on standard expressions for transmural transport and on solute and water conservation. Model results suggest that the preferential interactions among tubules enhance the urine concentration capacity of short medullary cones by reducing the diluting effect of the descending limbs on the region of the interstitium where the collecting ducts are located; however, the effects on longer cones are unclear.

Keywords: kidney, bird, Japanese quail, renal medulla, differential equations.

1 Introduction

The avian kidney, like the mammalian kidney, can regulate blood plasma osmolality. When deprived of water, the urine concentrating mechanism (UCM) in the avian renal medulla stabilizes the osmolality of blood plasma by producing a hypertonic urine, i.e., a urine that is more concentrated than blood plasma. Localized in the medullary cone, the UCM raises urine osmolality by absorbing from the collecting ducts (CDs) more water than solute into the vasculature of the medulla, thereby increasing the osmolality of the CD fluid—fluid that is called urine after it emerges from the CDs. Based mostly on transepithelial transport properties of the Japanese quail, Nishimura et al. proposed that the avian UCM functions as a countercurrent multiplier [19]: water absorption from CDs is driven by active transepithelial transport of NaCl from the thick ascending limbs (ALs) into the surrounding interstitium, producing a “single effect”. The NaCl absorbed promotes, via osmosis, water absorption from CDs, descending limbs (DLs), and some blood vessels. The countercurrent configuration of renal tubules and blood vessels in the medulla augments this concentrating effect, as a function of depth, along the cortico-medullary axis: in a process called “countercurrent multiplication,” an osmolality gradient is generated along all structures of

the medulla, from the cortico-medullary boundary to the medullary tip.

Layton and collaborators confirmed, using a mathematical model, that the avian UCM operates as a countercurrent multiplier [15]. Their model represents loops of Henle and a CD system, which interact through a common compartment, the central core. The central core represents all structures within the medulla but external to the loops of Henle and CDs, e.g., the interstitial spaces, the interstitial cells, and the vasculature [24]. This central core formulation assumes that all medullary structures are uniformly distributed. However, Nishimura et al. have shown that the organization of the tubules and vessels in the medullary cone, especially the lower half, of the quail is highly structured [19]. A prominent ring of CDs surround a core of thin limbs and capillaries, with thick limbs scattered inside the core and in the peripheral regions.

A principal goal of this study is to investigate the role, in the context of the UCM, of the structural organization revealed by Nishimura et al. [19]. To this end, we develop a mathematical model of the avian UCM that represents potential preferential interactions among tubules. We follow the “region-based” approach used by Layton and Layton in models of the outer medulla of the rat kidney [10, 12]. In that approach, “concentric regions” are used to

represent radial positions of tubules and vasa recta; tubules and vasa recta that are separated by at least a layer of tubules or vasa recta are assigned to different concentric regions. Vasa recta are explicitly represented in [10, 12]. However, the physical and transport properties of the vasa recta are not well characterized in the avian kidney. Thus, we combine the central core formulation with the region-based approach, and we represent in this model an inner central core and an outer central core (or, two “concentric cores”), by which the vasculature is implicitly represented. The radial positions of the tubules are specified via their assignments to the two concentric cores. Model results suggest that in small medullary cones structural organization (or, regionalization) can increase urine osmolality, without reduction in free water absorption.

2 Model formulation

In the avian kidney, loops of Henle are of differing lengths and turn back at differing levels along the medullary cone, with most turning back near the cortico-medullary boundary. This configuration can be represented in the model by means of continuously distributed loops [13]; see Fig. 1. In a

distributed-loop model, tubular concentration profiles in loops turning at differing levels are assumed to be different, and transmural fluxes are weighted according to the number of loops turning at each level. The fraction of loops reaching to level y is denoted by $w(y)$:

$$w(y) = \begin{cases} e^{-3.22y/L}, & y \in [0, L] \\ 0, & \text{otherwise,} \end{cases} \quad (1)$$

where L denotes the length of the medulla.

We assume that there are n_L loops of Henle and n_{CD} CDs. Along the medullary cone, the CDs repeatedly coalesce, with two CDs joining to become one at each coalescence. Thus, the CD population decreases approximately exponentially. In the model, all CDs are merged into a single composite tubule, and the effect of the coalescences is represented by decreasing tubular area as a function of increasing medullary depth. Specifically, the CD radius is scaled by a factor of $e^{-2.8x/L}$ [15].

Two concentric cores are represented to simulate the potential preferential interactions among tubules that are suggested by anatomical studies [19]. The outer and inner cores are denoted CC_O and CC_I , respectively. The loops of Henle and CDs interact within the concentric cores. Tubules that are separated by at least a layer of tubules or vasa recta are assigned to different

concentric cores. By assigning each tubule to a concentric core, or, in case of the AL, a fraction of the tubule to each of the two concentric cores, the relative positions or distributions of the tubules can be represented. Tubules entirely assigned to different cores may still have limited interaction because solutes may diffuse around the tubules. These diffusive fluxes are simulated by assigning nonzero permeabilities to the boundaries between concentric cores.

Because NaCl is believed to be the only solute that plays a significant role in the avian UCM [3, 23], the model is formulated for a single solute, represented by Na^+ and indexed by the subscript s . Osmolalities were computed by assuming that Na^+ was accompanied by an anion, assumed to be principally Cl^- . Water is indexed by the subscript V . The DLs, ALs, CD are represented by rigid tubules (indexed by $i = 1, 2$, and 3 , respectively). CC_O and CC_I are also represented by rigid tubules (indexed by $i = 4$ and 5). All tubules extend in space from $x = 0$ (top of the cortex) to $x = L$ (medullary tip). An additional variable, $y \in [0, L]$, indexes the level at which a loop of Henle turns.

2.1 Model equations

Model equations represent the conservation and transmural transport of solutes and water. The water flow rate at time t and position x in a DL or AL reaching to level y is denoted by $F_{iV}(x, y, t)$, and the transmural water line flux (i.e., the water transport rate per unit tubular length) is denoted by $J_{iV}(x, y, t)$, taken positive for transport into a tubule. With this notation, water conservation for a DL or an AL reaching to level y ($i = 1$ or 2), or a CD is represented by

$$\frac{\partial}{\partial x} F_{iV}(x, y, t) = J_{iV}(x, y, t), \quad (2)$$

$$\frac{\partial}{\partial x} F_{3V}(x, t) = J_{3V}(x, t). \quad (3)$$

Solute conservation in a DL, an AL, or a CD is represented by

$$\frac{\partial}{\partial t} C_i(x, y, t) = \frac{1}{A_i(x, y)} \frac{\partial}{\partial x} \left(-F_{iV}(x, y, t) C_i(x, y, t) + J_{is}(x, y, t) \right), \quad i = 1, 2 \quad (4)$$

$$\frac{\partial}{\partial t} C_3(x, t) = \frac{1}{A_3(x)} \frac{\partial}{\partial x} \left(-F_{3V}(x, t) C_3(x, t) + J_{3s}(x, t) \right), \quad (5)$$

where C_i is the solute concentration of a tubule i , A_i is the cross-sectional area, and J_{is} is the transmural solute line flux, taken positive into the tubule.

Transepithelial transport was represented by a single barrier formulation. Driven by the transmural osmolality difference, transmural water flux into a

DL, an AL, or a CD is given by

$$J_{iV}(x, y, t) = 2\pi r_i(x, y) P_{f,i}(x, y) \bar{V}_w \phi \left(C_i(x, y, t) - (\kappa_{i,4} C_4(x, t) + \kappa_{i,5} C_5(x, t)) \right),$$

$$i = 1, 2 \quad (6)$$

$$J_{3V}(x, t) = 2\pi r_3(x) P_{f,3}(x) \bar{V}_w \phi \left(C_3(x, t) - (\kappa_{i,4} C_4(x, t) + \kappa_{i,5} C_5(x, t)) \right).$$

$$(7)$$

where r_i is the radius of a tubule, $P_{f,i}$ is the transmural osmotic water permeability coefficient, \bar{V}_w is the partial molar volume of water (0.018136 cm³/mmole at 37°C, see p. B-152 and p. F-5 in [26]), and ϕ is the osmotic coefficient of NaCl, 1.84 [26]. Reflective coefficients normally appear as part of the products on the right-side of (6) and (7), but we assume that all reflection coefficients equal one, as is thought to be the case in mammalian tubules [22]. The relative position of a tubule i is specified by the parameters $\kappa_{i,4}$ and $\kappa_{i,5}$, which denote the fractions of the tubule i that are in contact with CC_O and CC_I , respectively; thus, $\kappa_{i,4} + \kappa_{i,5} = 1$. The transmural fluxes from a tubule i into CC_O and CC_I are scaled by $\kappa_{i,4}$ and $\kappa_{i,5}$, respectively.

The transmural solute flux into a DL, an AL, or a CD is given by

$$J_{is}(x, y, t) = 2\pi r_i(x, y) \left(P_i(x, y) \left(\kappa_{i,4} C_4(x, t) + \kappa_{i,5} C_5(x, t) - C_i(x, y, t) \right) + \frac{V_{\max,i} C_i(x, y, t)}{K_{m,i} + C_i(x, y, t)} \right), \quad (8)$$

$$J_{3s}(x, t) = 2\pi r_3(x) \left(P_3(x) \left(\kappa_{i,4} C_4(x, t) + \kappa_{i,5} C_5(x, t) - C_3(x, t) \right) + \frac{V_{\max,3} C_3(x, t)}{K_{m,3} + C_3(x, t)} \right). \quad (9)$$

where P_i is the solute permeability of tubule i , $V_{\max,i}$ is the maximum transport rate per unit tubular area for metabolically-drive active transport, which is assumed to have the form of Michaelis-Menten kinetics with Michaelis constant $K_{m,i}$.

We assume that a fraction, β , of the net fluid accumulation in CC_O ($i = 4$), arising from water absorption from tubules, is shunted, as capillary flow, to the CC_I ($i = 5$); the rest of the net fluid accumulation in CC_O is assumed to be taken up by ascending vasa recta (and contributes to axial flow in CC_O). Thus, water and solute conservation for the concentric cores is given by

$$\frac{\partial}{\partial x} F_{4V}(x, t) = (1 - \beta) J_{4V}(x, t) \quad (10)$$

$$\frac{\partial}{\partial x} F_{5V}(x, t) = \beta J_{4V}(x, t) + J_{5V}(x, t) \quad (11)$$

$$\frac{\partial}{\partial t} C_4(x, t) = \frac{1}{A_4(x)} \frac{\partial}{\partial x} \left(-F_{iV}(x, t) C_4(x, t) + (1 - \beta) J_{4s}(x, t) \right), \quad (12)$$

$$\frac{\partial}{\partial t} C_5(x, t) = \frac{1}{A_5(x)} \frac{\partial}{\partial x} \left(-F_{5V}(x, t) C_5(x, t) + \beta J_{4s}(x, t) + J_{5s}(x, t) \right). \quad (13)$$

The transmural water and solute fluxes into the concentric cores arise from the total transmural fluxes of the loops and CD. The total transmural flux $\bar{J}_{ik}(x, t)$, where $k = s$ or V , from the DLs or ALs ($i = 1$ or 2) at level x is given by an integral of the fluxes from loops turning at level x or beyond, weighted by the rate at which the loops turn, i.e., by $-w'(y) \equiv -dw(y)/dy$:

$$\bar{J}_{ik}(x, t) = J_{ik}(L, L, t) + \int_x^L J_{ik}(x, y, t)(-w'(y)) dy. \quad (14)$$

The equations of transmural water and solute fluxes for the CC are given by

$$J_{4k}(x, t) = -\left(\bar{J}_{1k}(x, t) + \bar{J}_{2k}(x, t) + \frac{n_{\text{CD}}}{n_{\text{L}}} J_{3k}(x, t)\right). \quad (15)$$

2.2 Boundary conditions

To complete the system, we specify boundary conditions for the DLs and CD at $x = 0$, and for the ALs and CC at $x = L$.

For the DLs, $F_{1V}(0, y, t)$ and $C_1(0, y, t)$ must be specified for $t \geq 0$. We assume that $C_1(0, y, t) = C_p = 156$ mM, and that at the cortico-medullary boundary DL inflow rate increases linearly as the loop length increases. That is,

$$F_{1V}(0, y, t) = \left((1 - \gamma)\frac{y}{L} + \gamma\right) F_{V,o}, \quad (16)$$

where $F_{V,o}$, which denotes the fluid flow of longest DL at the cortico-medullary

boundary, is set to 4.42 nl/min, and $\gamma = 0.84$.

At each loop bend, each DL is contiguous with an AL; thus, $F_{2V}(y, y, t) = -F_{1V}(y, y, t)$, where the flow is taken positive in the increasing x direction; and $C_2(y, y, t) = C_1(y, y, t)$.

Boundary conditions are also required for the CD at $x = 0$. We estimate CD water inflow by

$$F_{3V}(0, t) = -\frac{n_L \alpha \bar{F}_{2s}(0, t)}{n_{CD} C_3(0, t)}, \quad (17)$$

where α is set to 0.11 so that at steady state $F_{3V}(0)$ is approximately 0.5 nl/min per nephron [15]. \bar{F}_{2s} is the total solute flow at the cortico-medullary boundary from ALs, given by

$$\bar{F}_{2s}(0, t) = F_{2s}(0, L, t) + \int_0^L F_{2V}(0, y, t) C_2(0, y, t) (-w'(y)) dy. \quad (18)$$

In the base case, CD boundary solute concentration is assumed to be that of plasma; i.e., $C_3(0, t) = C_p$.

The concentric cores are assumed to be closed at $x = L$, which implies that there is no advective entry of solute or fluid at $x = L$; thus, $F_{4V}(L, t) = F_{5V}(L, t) = 0$.

2.3 Model parameters

We assume that there are 98 loops of Henle and 28 CDs [15]; thus, $n_L = 98$ and $n_{CD} = 28$. The length of the medullary cone L is taken to be 3.25 mm [15]. The diameters and transport properties of the tubules are shown in Table 1. NaCl permeabilities are given by the harmonic mean [6] of the permeabilities of individual ions. The model DL is structurally and functionally divided into two segments. The first segment is a thin-walled segment that has high water and NaCl permeabilities. The second segment is a terminal segment, which we call the prebend segment of length 255 μm (as computed by Layton et al. [15] for cone 11 in [2]) and which is assigned the diameter and transport properties of the thick AL. CD NaCl permeability is based on NaCl permeability in rabbit outer medullary CD [25]. Cell types are assumed to change abruptly along the DL; thus, e.g., $P_{f,1}(x) = 546 \mu\text{m}$ for $0 \leq x \leq 255 \mu\text{m}$, and $P_{f,1}(x) = P_{f,2}(x) = 56.6 \mu\text{m}$ for $255 \mu\text{m} < x \leq L$; similarly, $P_{1s}(x)$ and $V_{\max,1}(x)$ are also discontinuous functions. The DL radius is smoothly interpolated from the thin DL to the prebend segment as in [17].

The solute permeabilities of the boundaries of the concentric cores are given by $P_{4s} = D_s / (N_B \Omega \tau r)$, where $N_B = 28$ denotes the number of nephrons per bundle, $\Omega = 0.1$ is a diffusion resistance that represents effects of macro-

molecules and interstitial cells present in the interstitium and the fraction of the core boundary (i.e., circumference fraction) available for diffusion, and where τ represents the effect of tortuosity on diffusion path length around tubules and vessels. The path around the periphery of a tube is about $\pi/2$ greater than a direct path, and thus we take $\tau = \pi/2$. The distance between the center of the inner core to the midpoint between the perimeters of the two cores is $r = 87.5 \mu\text{m}$. With the specified values for N_B , r , Ω , and τ , one obtains $P_{4s} = 4.18 \times 10^{-6} \text{cm/s}$.

The relative positions or distributions of the tubules, specified by the parameters $\kappa_{i,4}$ and $\kappa_{i,5}$, are shown in Fig. 2. By definition, $\kappa_{i,5}$ is given by $1 - \kappa_{i,4}$. The distributions of the DL and AL are different. Because the model DL and AL are assumed contiguous at the loop bend, their position parameters are equal at each loop bend; i.e., one should have $\kappa_{1,4}(x, x) = \kappa_{2,4}(x, x)$. To achieve this, the prebend of the model DL moves away from CC_I to reach the AL, which is closer to the CD. That is, near the loop bend, the DL position parameters change gradually from $\kappa_{1,4} = 1$ and $\kappa_{1,5} = 0$ to $\kappa_{1,4} = 0.2$ and $\kappa_{1,5} = 0.8$, using a cubic spline as in [12].

2.4 Numerical method

Steady-state solutions to model equations (2)–(13) are computed using the SLSI-Newton method. In the SLSI-Newton method, the semi-Lagrangian semi-implicit (SLSI) scheme generates an approximate steady-state solution using a large time step. This intermediate solution is then used as an initial guess for the Newton solver, which generates a more accurate steady-state solution by solving the steady-state formulation of the model equations. Details of the method can be found in [8, 9].

All computations reported below were performed using Fortran programs implemented in double precision on a computer system with a 3.2 GHz Pentium IV processor and 1 GB of RAM. A spatial discretization of 160 subintervals were used.

3 Model results

Base-case results. Figure 3 shows osmolality profiles for the longest loop of Henle, the CD, the central core for the radially homogeneous case (i.e., one concentric core represented, which we call “case 1,” panel A), and the concentric cores for the radially distributed case (which we call “case 2,” panel

B). We let CC (no subscript) denote the central core in case 1, which corresponds to the standard central core formulation. In both case 1 and case 2, all tubules (except along the prebend segment) exhibit an increasing osmolality gradient along the cortico-medullary axis. This osmolality gradient is maintained by active, outward-directed transepithelial transport of NaCl of the thick limbs. The osmolality of the intratubular fluid in the prebend segment of the DLs and in the ALs is progressively reduced along the flow direction by the active transport of NaCl. The NaCl absorbed from the prebend segments and ALs raises osmolalities in the DLs, CD, and concentric cores.

Near the medullary cone tip, interstitial fluid osmolalities in CC, CC_I , and CC_O exhibit a plateau corresponding to the location of the prebend segment of the longest loop. Within this plateau region, fluid osmolality is highest in CC_I , where the low water permeability of the prebend segments limits their diluting effect on the interstitium; fluid osmolality is higher in CC than in CC_O , because in case 1 the CC fluid osmolality is raised by NaCl transported out of all the prebend segments and the thick ALs, whereas only 80% of that NaCl is directed to CC_O . Outside of this plateau region (i.e., before the beginning of the prebend segment of the longest loop), CC_O has the highest fluid osmolality, because it is in contact with 80% of the ALs

and prebend segments, and because it is not diluted by water absorbed from the DLs. Because the solute permeability of the boundary between the two concentric cores are finite, the osmolality of CC_I lags that of CC_O at each medullary level outside of the plateau region.

The osmolality difference between CC_O and CC is at its maximum at the cortico-medullary boundary, and this difference gradually decreases along the medullary axis. This trend can be attributed to the competing effects of regionalization—a concentrating effect and a diluting effect on the UCM. Near the cortico-medullary boundary, the separation of DLs from CD introduces a concentrating effect by reducing the diluting effect of the DLs on CC_O ; this raises CC_O (and thus CD) osmolality. However, the separation of the majority of the ALs from CC_I also introduces a diluting effect. CC_I osmolality is lowered, which in turn lowers DLs fluid osmolality. This results in lower prebend segment and AL fluid osmolalities, and thus reduced NaCl transmural fluxes into CC_O . Because any concentrating effect is augmented by the countercurrent loop configuration, the difference in loop-bend osmolality between case 1 and case 2, taken in isolation, would increase away from the cortex. In other words, the impact of the reduced NaCl fluxes (i.e., the diluting effect of regionalization) becomes progressively more important,

compared to its concentrating effect, as one approaches the medullary cone tip. As a result, the difference between fluid osmolalities in CC_O and CC , or in the two CDs, becomes progressive smaller.

Because the solute concentration (and thus osmolality) of CC_I is lower than that of CC , except where the fluid osmolality of each core exhibits a plateau, the solute concentration in DLs, which are located in CC_I , is lower in case 2 than in case 1, at each medullary level. However, because the solute concentration of CC_O , where the ALs are located, is higher than that of CC (again outside of the plateau region), solute back-fluxes into the ALs are larger in case 2 than in case 1. Thus, where sufficiently far from the loop bend, AL solute concentration is higher in case 2 than in case 1.

Except where the interstitial fluid osmolality exhibits a plateau, CC_O osmolality is higher than CC ; consequently, CD fluid osmolality is higher in case 2 than in case 1. A direct comparison of the two CD profiles is included in Fig. 4 (the two curves labeled “Base case”). At the cortico-medullary boundary, CD fluid osmolality is set to plasma osmolality in both cases. Because of the higher interstitial osmolality in CC_O , CD fluid osmolality rises more rapidly in case 2 than in case 1, with the difference reaching its maximum at $x \approx 1300 \mu\text{m}$. This difference then gradually decreases, as the osmolality

difference between CC_O and CC decreases and eventually reverses, until at $x > 3120 \mu\text{m}$, CD fluid osmolality in case 1 exceeds that in case 2 by 4.2 mosmol/(kg H_2O), or a relative osmolality difference of $4.2/(686-287) = 1\%$. (Blood plasma osmolality is assumed to be 287 mosmol/(kg H_2O).)

Variation in medullary cone length. Given how regionalization affects the concentrating capability differently at varying medullary cone depth, a reasonable question, then, is how are model results affected by variation in medullary depth? Indeed, the experimentally measured cone length in quail ranges from 950 to 3350 μm . Our base-case cone length of $L = 3250 \mu\text{m}$ is close to the upper bound of the measurement. (A large cone is used because of the availability of anatomical measurements for this particular cone [15].) Thus, we assess the regionalization effects on the UCM of a short cone. Figure 4 shows CD fluid osmolality profiles obtained in case 1 and case 2, for the base case and for a short cone ($L = 950 \mu\text{m}$). Parameters for this short cone are set to base-case values; the prebend segment is assigned the normalized length of the base case, i.e., $255 \mu\text{m} \times 950/3250 = 74.54 \mu\text{m}$ (this gives a fixed prebend-to-medullary length ratio in both cones). Because the concentrating effect of the NaCl active transport is augmented

by the countercurrent configuration of the renal tubules, the longer the cone, the larger the concentrating effect, i.e., the higher the urine osmolality, or, in fact, the higher the CD fluid osmolality at each *normalized* medullary depth (normalized by cone length).

Recall that our base-case results indicate that the diluting effect of regionalization (via reduced AL NaCl fluxes) is increased with increasing medullary cone depth. Thus, throughout the short cone, the diluting effect is less important compared to the concentrating effect of regionalization. As a result, for the short cone, the difference in CD fluid osmolality between case 1 and case 2 increases along the cortico-medullary axis. Urine osmolalities for cases 1 and 2 are 357 and 395 mosmol/(kg H₂O), respectively. The osmolality difference of 38 mosmol/(kg H₂O) corresponds to a relative osmolality increase of $38/(357-287) = 54.29\%$.

Because a key motivation behind mathematical models of the UCM is to explain the production of hypertonic urine, we have so far reported only osmolality. However, as noted in [5, 17, 27], the effect of UCM on blood plasma osmolality is more accurately measured by the free-water absorption rate (FWA). FWA is the volume, per unit time, of blood plasma that could be considered to be completely cleared of solute by the production of a urine

that is more concentrated than blood plasma; FWA is given by

$$F_{3V}(L, t) \left(\frac{C_3(L, t)}{C_p} - 1 \right) \quad (19)$$

We consider the effect of regionalization on urine osmolality, FWA, and urine flow rate, for differing medullary cone lengths. Results are shown in Fig. 5. As noted previously, longer cones yields more concentrated urines because of countercurrent multiplication, and for sufficiently short cones, regionalization results in a more concentrated urine. The difference in urine osmolality between case 1 and case 2 (labeled “No region” and “With regions,” respectively) gradually decreases as cone length is increased, until at $L > 3160 \mu\text{m}$, the diluting effect of regionalization exceeds that of its concentrating effect, and a less concentrated urine is obtained in case 2. Note that this critical depth is near the upper bound of the measured cone lengths, so for most cones regionalization raises urine osmolality. As L is increased from 950 to 3350 μm , urine flow rate decreases from 0.4869 to 0.2189 nl/min in case 1, and from 0.4284 to 0.2168 nl/min in case 2. The competing effects of urine osmolality increase and flow rate decrease result in increasing FWA, with decreasing slope, in both cases. Regionalization results in a higher FWA for $L < 2860 \mu\text{m}$.

Variation in prebend length. In all previous simulations, the normalized prebend length is fixed for all cone sizes, which implies a shorter prebend segment for a shorter cone. However, Casotti et al. found minimal correlation between prebend length and loop length [2]. Thus, in another set of simulations, we set the dimensional prebend length of the short cone to the base-case value of $255 \mu\text{m}$. Figure 6 shows CD fluid osmolality profiles obtained with and without regionalization, for the base-case cone and for the short cone ($L = 950 \mu\text{m}$). These results are similar to those shown in Fig. 4. (In fact, the base-case profiles are the same as those in Fig. 4.) Longer prebend segments increase the concentrating capability of the short cone: urine osmolality is 418 and 438 mM in case 1 and case 2, respectively (compared to 357 and 395 mM in case 1 and case 2, respectively, obtained previously with fixed normalized prebend length). Thus, the urine osmolality difference between case 1 and case 2 is 20 mosmol/(kg H₂O) in this short cone, or a relative osmolality increase of 15% (which is less than the difference of 30 mosmol/(kg H₂O) with fixed normalized prebend length). The comparison, between case 1 and case 2, for urine osmolality, FWA, and urine flow rate as functions of medullary cone lengths is also qualitatively similar to Fig. 5 (data not shown). These results suggest that the concentrating

effect of regionalization in short cones is reduced, but still significant, with longer prebend segments.

Concentric core boundary permeability. The solute permeability between CC_O and CC_I is based on estimates of diffusion resistance arising from macromolecules and interstitial cells in the interstitium, tortuosity of diffusion path around tubules, and the spaces between tubules, none of which has been well characterized. The degree of regionalization increases as the region boundary permeability decreases. In a sensitivity study, the base-case boundary solute permeability is scaled by factors of $p = 0.1, 0.5, 1, 2, 10,$ and 100 ; $p = 0.1$ corresponds to greatest regionalization, $p = 100$ corresponds to least regionalization, and $p = 1$ corresponds to the base case.

CD fluid osmolality profiles for these incremental degrees of regionalization and for case 1 are shown in Fig. 7. As regionalization is decreased by increasing p from 0.1 to 100, CD osmolality increasingly approximates case 1, while CC_O and CC_I becomes more nearly one well-mixed core (results not shown). Although the urine osmolality is increased by a higher degree of regionalization, the effect is modest.

Reduced regionalization near cortex. Some experimental studies have suggested that the structural organization of tubules is less well-defined near the cortico-medullary boundary [19]. To assess the effect of axial variation in regionalization, we obtained model results where boundary permeability is higher near the cortico-medullary boundary. The effective solute permeability between CC_O and CC_I is represented by

$$P_{4s}(x) = \begin{cases} (10 - 9\frac{x}{d}) P_0, & 0 \leq x < d \\ P_0, & d \leq x \leq L \end{cases} \quad (20)$$

where P_0 denotes the base-case solute permeability of the CC_O and CC_I boundary.

CD osmolality profiles are shown in Fig. 8 for $d = 0$ (base case), 0.2, 0.4, 0.6, 0.8, and 1, and for case 1. Results are obtained for the base-case medullary length (panel A) and for a short cone $L = 950 \mu\text{m}$ (panel B). For the base-case cone length, near the cortico-medullary boundary, the base-case CD osmolality ($d = 0$) is the highest because of the initial concentrating effect of regionalization, as explained previously. Near the medullary cone tip, the diluting effect of regionalization becomes increasingly important, and CD osmolality profiles for case 1 and for $d > 0$ exceed that for the base case. Indeed, urine osmolality is higher for $d = 0.4, 0.6,$ and 0.8 than for case 1,

although the difference is small. (The largest urine osmolality difference for these cases, which is between $d = 0.4$ and case 1, is 7 mosmol/(kg H₂O).)

Results for the short cone is more straightforward: CD osmolality decreases as d is increased. Nonetheless, the concentrating effect of regionalization is not completely abolished by the reduced degree of regionalization near the cortex. For $d = 0.4$, a urine osmolality of 379 mosmol/(kg H₂O) is obtained, which corresponds to a relative osmolality increase of $(379-357)/(357-287) = 31.42\%$.

Capillary flow. The distribution of capillary flow in the avian medullary has not been characterized, so we made assumptions that appear to be physiologically reasonable. We assumed that 80% of the net fluid accumulation in CC_O is shunted as capillary flow to CC_I , whereas the rest is taken up by ascending vasa recta in CC_O . To assess the impact of vessel and capillary distribution, we conducted simulations for $\beta = 0, 0.2, 0.4, 0.6, 0.8,$ and 1. In the base case, $\beta = 0.8$; a smaller β implies less trans-core flow. Figure 9 shows CD osmolality profiles obtained for these values of β and for case 1.

CC_I osmolality is raised by outward-directed active NaCl transport from a fraction of the prebend segments, by solute diffusion from the more concen-

trated CC_O , and by the trans-core flow from CC_O . Thus, as β decreases from 1 to 0, this trans-core flow decreases, thus lowering CC_O osmolality. This also results in lower DL osmolality, reduced NaCl fluxes from the prebend segments and ALs, and finally a reduced concentrating capacity.

4 Discussion

We have developed a mathematical model framework for the renal medulla of the quail kidney. The model includes distributed loops of Henle and a composite CD. To represent the structural organization of renal tubules revealed by some anatomic studies, the model uses a modified central core formulation: by representing two concentric cores and by assigning fractions of tubules to each concentric core, the model represents the relative positions of renal tubules and simulates their preferential interactions. The model predicts that such preferential interactions improve the concentrating capability of medullary cones that are sufficiently short, but the effect on longer cones is unclear.

Because the avian UCM depends on a countercurrent flow configuration of the renal tubules, a configuration that augments the concentrating effect

along the cortico-medullary axis, the concentrating capacity of a longer cone exceeds that of a shorter one. This difference is highlighted in an optimization study by Marcano et al. [16]. In that study, they varied model morphological and transport parameters within specified ranges to maximize FWA, for medullary cones of various sizes. For a short cone of $950\ \mu\text{m}$, the urine osmolality corresponding to a maximum FWA is $362\ \text{mosmol}/(\text{kg H}_2\text{O})$, whereas for their base-case cone of $3250\ \mu\text{m}$ it is $597\ \text{mosmol}/(\text{kg H}_2\text{O})$. (The corresponding urine osmolalities predicted by our model without regionalization are 357 and $686\ \text{mosmol}/(\text{kg H}_2\text{O})$, respectively, although model assumptions such as CD boundary conditions differ between our model and that of [16], so strictly speaking these results are not comparable.) Thus, the structural organization in the avian medullary cone may have been developed to provide the best benefits for shorter cones.

The results of this study illustrate the importance of representing the radial distribution of tubules in models of the UCM. When this distribution is not represented, our model underestimates the concentrating capability, measured by urine osmolality increase over plasma, by $\sim 50\%$ for a short cone. Although our model predicts minimal impact of structural organization in a longer cone on urine osmolality, tubular concentration profiles differ

significantly from those obtained with structural organization represented. It is possible that a more sophisticated model of the avian UCM, perhaps one that explicitly represents the vasculature, may reveal more important functions of the structural organization in long cones.

Like the avian medulla, the organization of tubules and vasa recta in the mammalian outer renal medulla is also highly structured [7]. In the outer medulla of the rat and several other mammals [1], tubules and vessels are found to be organized concentrically around vascular bundles, tightly packed clusters of parallel vessels and tubules containing mostly vasa recta. The regionalization in the rat outer medulla has been shown to play a significant role in urea sequestration in the vascular bundles [11]. The structural organization of tubules and vessels differs significantly among different mammalian species. In some species having high urine concentrating capability, the DLs of short loops of Henle are found at the periphery of the vascular bundles (e.g., rat) or within the vascular bundles (e.g., mouse); such bundles are called complex bundles. Those bundles containing only vasa recta (e.g., rabbit, golden hamster, or human) are called simple bundles [5]. The different degrees of regionalization among different mammals are not surprising given the difference in the diet of the animals, transepithelial transport properties

of these kidneys, etc. Indeed, the results of the present study suggest that the differing sizes of these kidneys, in particular, likely play a role in the effect of regionalization on their concentrating capacity.

The concentrating mechanism in both the quail kidney and the outer medulla of the mammalian kidney is well-established, by physiological experiments and theoretical investigation, to be driven by outward-directed active NaCl transport of thick ALs. In contrast, the concentrating mechanism in the inner medulla of the mammalian kidney, where the thin ALs lack sufficiently $\text{Na}^+\text{-K}^+\text{-ATPase}$, remains to be elucidated [14, 22]. The organization of tubules and vessels has also been shown to be highly structured near the outer-inner medullary boundary of the rat inner medulla [21]. There, CDs are grouped together in single clusters. DLs are positioned predominantly at the periphery of each individual CD clusters and are absent from within the cluster, whereas ALs are distributed near uniformly among the CDs and DLs [21]. Thus, interestingly, the organization of tubules and vessels in the rat inner medulla is topologically similar to that in the quail kidney. We believe that model studies that capture the preferential interactions arising from the structural organization in the rat inner medulla may provide a deeper understanding of the inner medullary concentrating mechanism.

Table 1: Tubular diameters and transport parameters.

Description	Symbol	Value
DL radius	r_1	3.41 μm [15]
AL radius	r_2	4.78 \rightarrow 5.74 μm [15]
CD radius	r_3	9.55 \rightarrow 33.35 μm [15]
CC_I radius	r_4	50 μm
CC_O radius	r_4	125 μm
DL water permeability	$P_{f,1}$	546 $\mu\text{m/s}$ [19]
AL water permeability	$P_{f,2}$	56.6 $\mu\text{m/s}$ [18]
CD water permeability	$P_{f,3}$	116 $\mu\text{m/s}$ [20]
DL NaCl permeability	P_{1s}	130×10^{-5} cm/s [19]
AL NaCl permeability	P_{2s}	3.06×10^{-5} cm/s [18]
CD NaCl permeability	P_{3s}	0.94×10^{-5} cm/s *
Concentric core boundary NaCl permeability	P_{4s}	0.418×10^{-5} cm/s *
DL NaCl active transport rate	$V_{\text{max},1}$	0 nmol \cdot cm $^{-2}$ \cdot s $^{-1}$ [19]
AL NaCl active transport rate	$V_{\text{max},2}$	19.5 nmol \cdot cm $^{-2}$ \cdot s $^{-1}$ [18]
CD NaCl active transport rate	$V_{\text{max},3}$	0 nmol \cdot cm $^{-2}$ \cdot s $^{-1}$ *
Michaelis constant	K_m	40 mM [4]

DL and AL, descending and ascending limbs, respectively, of loop of Henle; CD, collecting duct. AL and CD radii are given at $x = 0$ and $x = L$. Arrow (\rightarrow) indicates that the parameter is assumed to vary linearly as x increases.

*See text.

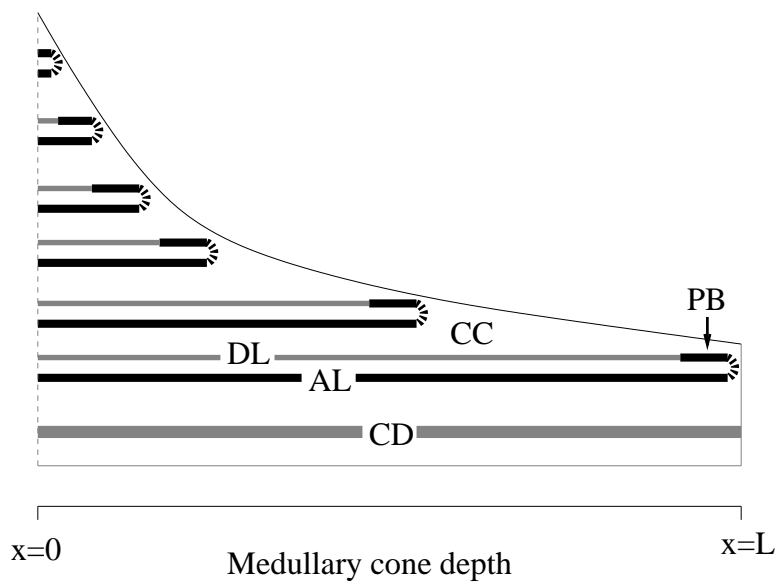


Figure 1: Schematic diagram of model loops of Henle and a composite CD. PB, prebend segment. Six representative loops are shown: however, the numerical formulation of the model uses 160 loops of Henle to approximate a continuously decreasing distribution.

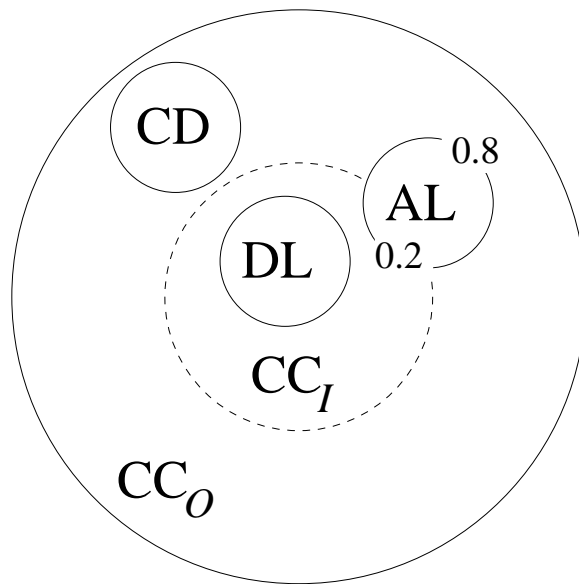


Figure 2: Relative position of tubules. The decimal numbers associated with the AL indicate relative weightings of interaction with CC_O and CC_I .

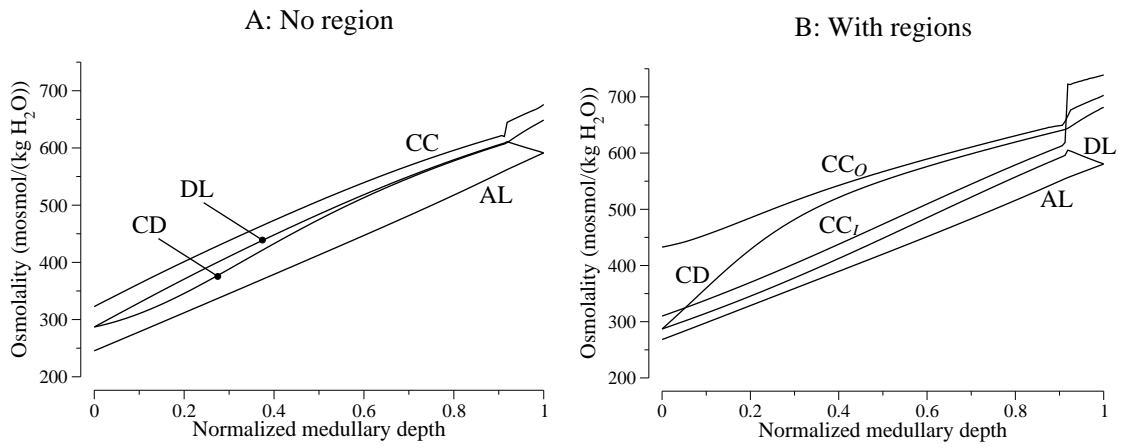


Figure 3: Profiles of tubule osmolality in longest loops of Henle (DL and AL), CD, CC (panel A), and CC_O and CC_I (panel B).

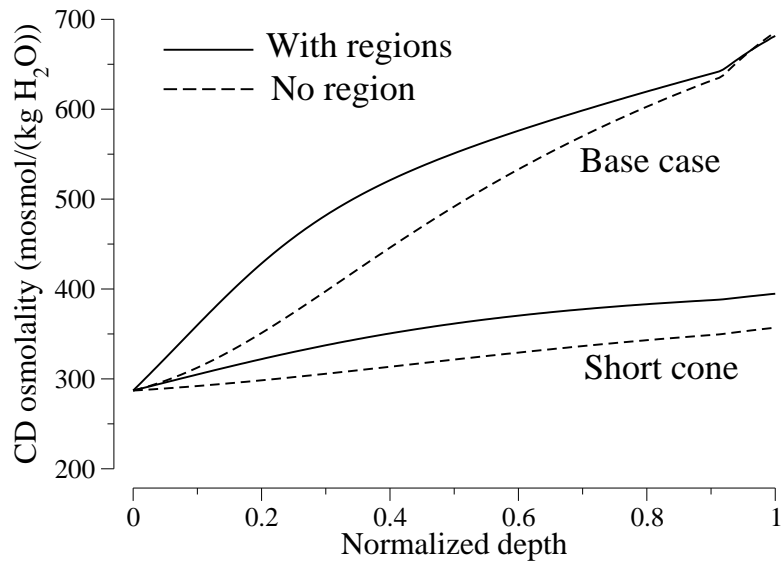


Figure 4: CD osmolality profiles. Solid line, with regionalization; dashed line, no regionalization. Base case, cone length $L = 3250 \mu\text{m}$; shrot cone, $L = 950 \mu\text{m}$.

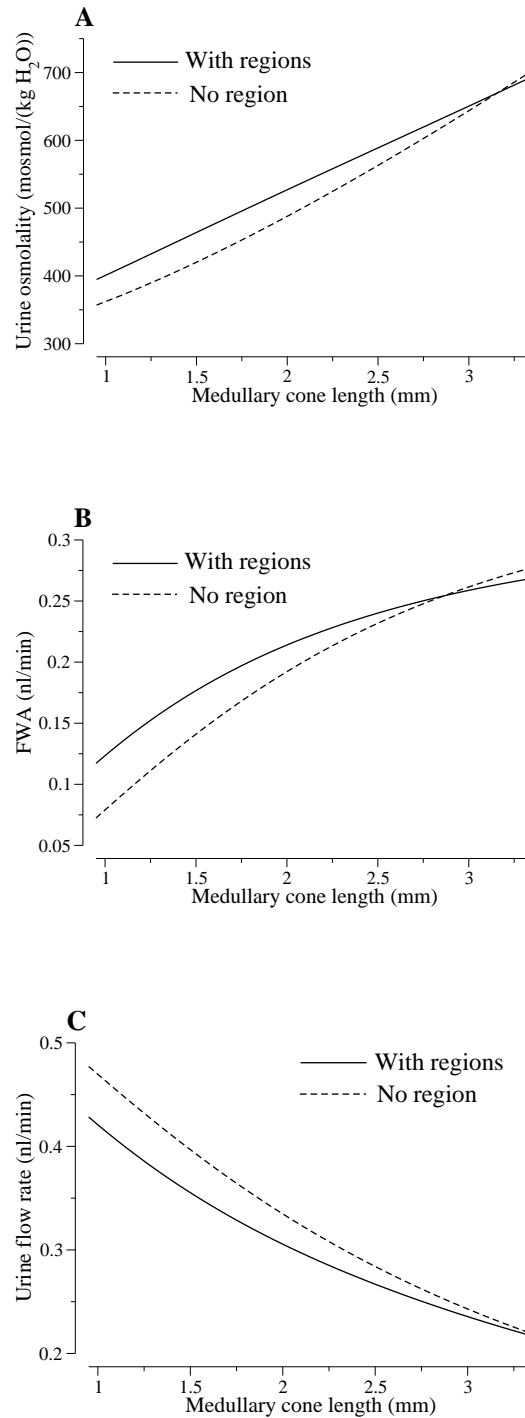


Figure 5: Effects of regionalization for differing medullary cone length, as evaluated in terms of urine osmolality (A), FWA (B), and urine flow rate (C). Solid line, with regionalization; dashed line, no regionalization. The concentrating effect of regionalization is significant for short cones, but di-

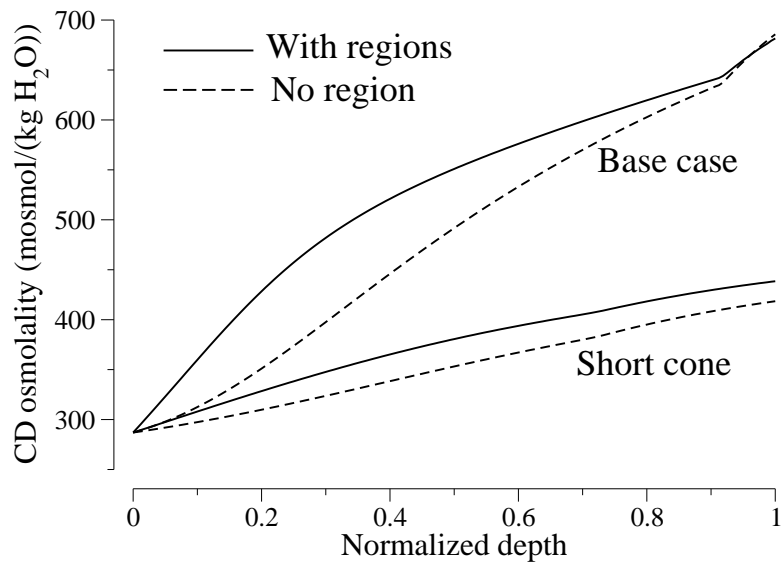


Figure 6: CD osmolality profiles. Notations are analogous to Fig. 4. Prebend length in short cone is longer than in Fig. 4.

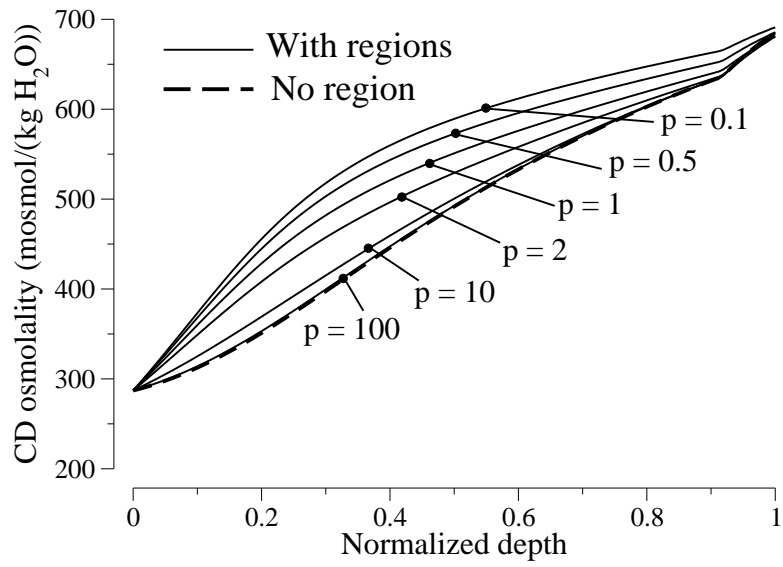


Figure 7: CD osmolality profiles obtained by scaling concentric core boundary permeability; the ratio of boundary solute permeability to base-case permeability is denoted by p .

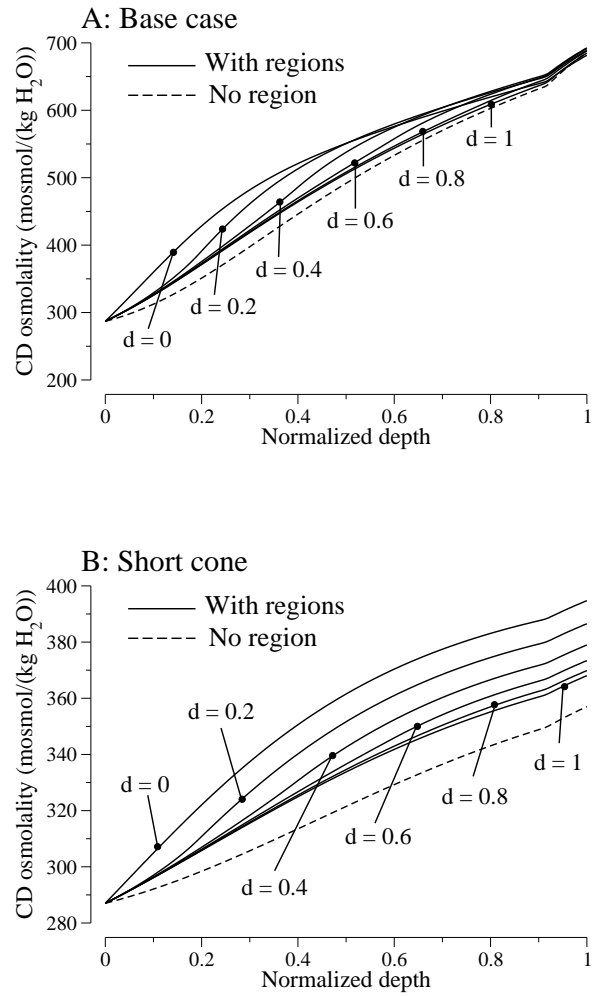


Figure 8: CD osmolality profiles obtained by varying the length of the upper medulla, denoted by d in normalized depth, where the degree of regionalization is reduced.

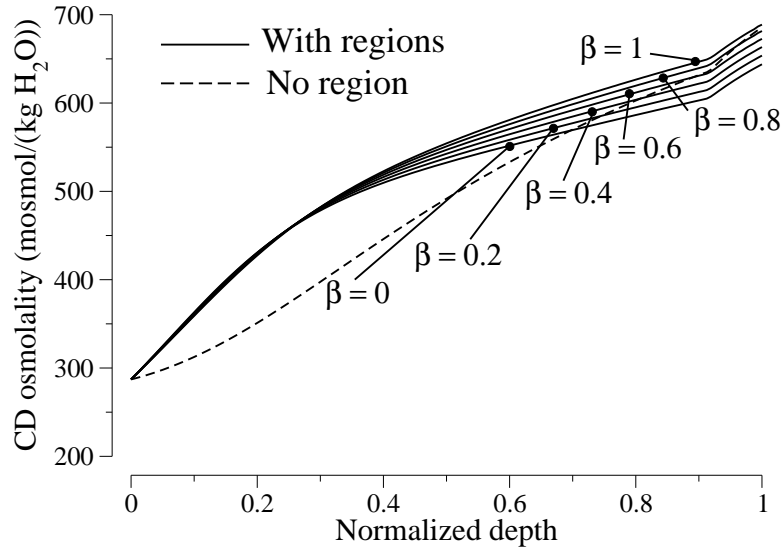


Figure 9: CD osmolality profiles obtained by varying fraction of net fluid accumulation in CC_O shunted to CC_I , denoted by β

References

- [1] L Bankir and C de Rouffignac. Urinary concentrating ability: insights from comparative anatomy. *Am J Physiol (Regulatory Integrative Comp Physiol 18)*, 249:R643–R666, 1985.
- [2] G Casotti, KK Lindberg, and Eldon J Braun. Functional morphology of the avian medullary cone. *Am J Physiol Regulatory Integrative Comp Physiol.*, 279:R1722–R1730, 2000.
- [3] N Emery, TL Poulson, and WB Kinter. Production of concentrated urine by avian kidneys. *Am J Physiol*, 223:180–187, 1972.
- [4] R Greger and H Velázquez. The cortical thick ascending limb and early distal convoluted tubule in the concentrating mechanism. *Kidney Int*, 31:590–596, 1987.
- [5] RL Jamison and W Kriz. *Urinary Concentrating Mechanism: Structure and Function*. Oxford University Press, New York, 1982.
- [6] O Kedem and A Leaf. The relation between salt and ionic transport coefficients. *J Gen Physiol*, 49:655–662, 1966.

- [7] W Kriz and B Kaissling. Structural organization of the mammalian kidney. In *The Kidney: Physiology and Pathophysiology*, pages 587–654, Philadelphia, 2000. Lippincott Williams & Wilkins.
- [8] AT Layton and HE Layton. An efficient numerical method for distributed-loop models of the urine concentrating mechanism. *Math Biosci*, 45(6):549–567, 2002.
- [9] AT Layton and HE Layton. A numerical method for renal tubules with abrupt changes in membrane properties. *J Math Biol*, 181(2):111–132, 2002.
- [10] AT Layton and HE Layton. A mathematical model of the urine concentrating mechanism in the rat outer medulla: I. Model formulation and base-case results. *Am J Physiol Renal Physiol*, submitted, 2003.
- [11] AT Layton and HE Layton. A mathematical model of the urine concentrating mechanism in the rat outer medulla: II. Parameter sensitivity and tubular inhomogeneity. *Am J Physiol Renal Physiol*, submitted, 2003.

- [12] AT Layton and HE Layton. A region-based model for the urine concentrating mechanism in the outer medulla of the rat kidney. *Bull Math Biol*, 65(5):859–901, 2003.
- [13] HE Layton. Distribution of Henle’s loops may enhance urine concentrating capability. *Biophys J*, 49:1033–1040, 1986.
- [14] HE Layton. Mathematical models of the mammalian urine concentrating mechanism. In *Membrane Transport and Renal Physiology, The IMA Volumes in Mathematics and Its Applications*, volume 129, pages 233–272, New York, 2002. Springer.
- [15] HE Layton, JM Davies, G Casotti, and EJ Braun. Mathematical model of an avian urine concentrating mechanism. *Am J Physiol Renal Physiol*, 279:F1139–F1160, 2000.
- [16] M Marcano, AT Layton, and HE Layton. An optimization algorithm for a distributed-loop model of an avian urine concentrating mechanism. *Bull Math Biol* (submitted), 2004.
- [17] M Marcano-Velázquez and HE Layton. An inverse algorithm for a mathematical model of an avian urine concentrating mechanism. *Bull Math Biol*, 65:665–691, 2003.

- [18] T Miwa and H Nishimura. Diluting segment in avian kidney II. water and chloride transport. *Am J Physiol Regulatory Integrative Comp Physiol*, 250:R341–R347, 1986.
- [19] H Nishimura, C Koseki, M Imai, and J Braun. Sodium chloride and water transport in the thin descending limb of Henle of the quail. *Am J Physiol Renal Physiol*, 257:F994–F1002, 1989.
- [20] H Nishimura, C Koseki, and TB Patel. Water transport in collecting ducts of Japanese quail. *Am J Physiol Regulatory Integrative Comp Physiol*, 271:R1535–R1543, 1996.
- [21] TL Pannabecker and WH Dantzler. Three-dimensional lateral and vertical relationship of inner medullary loops of henle and collecting duct. *Am J Physiol Renal Physiol*, 287:F767–F774, 2004.
- [22] JM Sands and HE Layton. Urine concentrating mechanism and its regulation. In Seldin DW and Giebisch G, editors, *The Kidney: Physiology and Pathophysiology*, pages 1175–1216, Philadelphia, 2000. Lippincott Williams & Wilkins.

- [23] E. Skadhauge and B. Schmidt-Nielsen. Renal medullary electrolyte and urea gradient in chickens and turkeys. *Am J Physiol*, 212:1313–1318, 1967.
- [24] JL Stephenson. Central core model of the renal counterflow system. *Kidney Int*, 2:85–94, 1972.
- [25] JB Stokes. Sodium and potassium transport across the cortical and outer medullary collecting duct tubule of the rabbit: evidence for diffusion across the outer medullary portion. *Am J Physiol Renal Fluid Electrolyte Physiol*, 242:F514–F520, 1982.
- [26] RC (ed.) Weast. *CRC Handbook of Chemistry and Physics*. CRC Press, Cleveland, 55 edition, 1974.
- [27] LG Wesson and WP Anslow. Effect of osmotic and mercurial diuresis on simultaneous water diuresis. *Am J Physiol*, 170:255–269, 1952.